Hindawi
Mathematical Problems in Engineering
Volume 2019, Article ID 7971594, 14 pages
https://doi.org/10.1155/2019/7971594

Research Article

Study on Adaptive Cruise Control Strategy for Battery Electric Vehicle

Sheng Zhang[1] **and Xiangtao Zhuan**[1,2]

[1]*School of Electrical Engineering and Automation, Wuhan University, Wuhan 430072, China*
[2]*Shenzhen Research Institute, Wuhan University, Shenzhen 518057, China*

Correspondence should be addressed to Xiangtao Zhuan; xtzhuan@whu.edu.cn

Received 2 September 2019; Revised 20 October 2019; Accepted 20 November 2019; Published 10 December 2019

Academic Editor: Leonardo Acho

This paper studies the control strategy for adaptive cruise control (ACC) system on a battery electric vehicle (BEV) in the car-following process, and the highlight of this paper is that the regeneration braking of BEV is considered in the car-following process. The hierarchical control structure is adopted for the ACC system. And the structure contains an upper controller and a lower controller. In the upper controller, multiple objectives including the safety, tracking, comfort, and energy consumption are optimized by using the model predictive control (MPC) method. In the lower controller, the energy is recovered during braking. So the energy economy is improved by reducing energy consumption and increasing energy recovery. The proposed ACC strategy is evaluated in simulation experiment. In the simulation experiment, safe tracking for the front vehicle is guaranteed, and the comfort and the energy economy are improved greatly. So the proposed adaptive cruise control strategy can make ACC more widely used in BEVs.

1. Introduction

With the increase in car ownership, the traffic accidents, environmental pollution, and oil shortage are getting worse [1]. To solve these problems, advanced driver-assistance systems (ADAS) and battery electric vehicles (BEVs) are two important vehicle technologies [2, 3].

Among various ADAS technologies, the adaptive cruise control (ACC) is an extension of traditional cruise control, which is used to improve the driving convenience and reduce the drivers' mental burden [4]. When there is no vehicle in front of a vehicle with ACC function (own vehicle), the own vehicle is on the state of speed control. When a vehicle (front vehicle) occurs in front of the own vehicle, the own vehicle is on the state of distance control, and the driving process of distance control is called the car-following process in this paper. During the car-following process, the own vehicle can ensure safety by tracking the velocity of front vehicle or keep an expected spacing [5].

BEVs use battery as energy source and motor as driving power source, so there are different dynamic characteristics and energy limitations compared with fuel vehicles [6–8]. The energy density of batteries for BEV is lower than conventional diesel and gasoline, which limits the distance traveled by BEV from the full charge [8]. And BEVs are charged for a long time, which puts higher demands for the distance traveled by BEV on one charge. Therefore, the improvement of the energy economy for BEV is necessary. And BEV with ACC function is selected as the research object in the paper. And the improvement of the energy economy for BEV is necessary. And multiple objectives of BEV during a car-following process including safety, tracking, comfort, and energy economy are optimized.

For the design of ACC controller, various control algorithms, that is, the sliding mode control, reinforcement learning, and fuzzy control algorithms, have been applied [9–12]. Among all kinds of control algorithms, model predictive control (MPC) is an algorithm that is commonly used for the study of ACC. The advantages of the MPC

algorithm can be summarized as follows: the optimization for control objectives is based on the model, so the process of modeling is convenient; various objectives can be integrated into an MPC framework, which can be easily handled by the designer; the various objectives are optimized in a method of online receding horizon optimization, which can compensate for errors due to inaccuracies in modeling [13–16].

Some studies related to the performance optimization of the ACC system for BEV have been done based on MPC. Madhusudhanan [8] proposed an efficient cruise control to improve driving range of the vehicle, where the speed reference for the own vehicle is obtained based on the upcoming traffic signal, while safety is guaranteed by maintaining a safe minimum spacing between two vehicles. Zhang et al. [17] proposed an energy efficiency control to increase driving range. And various traffic information was fully considered in the process of optimization. Schwickart et al. [18] proposed an ecocruise controller to minimize the energy consumption, and a compromise between the energy consumption and speed-reference tracking was achieved. Chen et al. [19] proposed a cruise controller, and energy consumption was reduced with terrain information based on the motor efficiency to increase the traveling distance. And the velocity is selected as the optimized variable for reducing the energy consumption.

For the regenerative braking, some researches have been finished. A sliding mode controller was designed to coordinate the antilock braking force and regeneration braking force by Bera et al. [20]. Kim et al. [21] applied the genetic algorithm to increase the braking energy recovery based on ensuring the vehicle stability, and the expected road friction coefficient and yaw moment were considered. Zhang et al. [22] designed a fuzzy controller for the braking energy recovery with the consideration of vehicle stability, and the simulation was performed in the ADVISOR platform. Xu et al. [23] designed the braking force distribution based on the ideal distribution curve. For increasing the braking energy recovery, the battery states and vehicle states were considered.

However, there are rare researches on combining ACC and braking energy recovery. This paper focuses on it. The contributions of this paper are that the braking energy recovery is considered in the car-following process and the energy economy during the car-following process is improved by reducing the energy consumption and improving the braking energy recovery.

2. BEV Model with Braking Energy Recovery

The front-wheel drive BEV is chosen as the modeling object, and the structure of the front-wheel drive BEV is shown in Figure 1. In the braking process, the motor drives the final drive to apply braking force to the front axle. Since the motor braking is affected by various factors, it is needed to make coordination for the hydraulic braking to complete the braking process. The hydraulic braking is implemented through controlling the hydraulic pressure adjustment unit of the electronic stability control (ESC) system. The vehicle model is designed in Carsim software, but the complete powertrain model of BEV is not included in Carsim, so the external models of motor and battery need to be added. The lithium battery and permanent magnet synchronous motor are selected for BEV in this paper.

The internal resistance model is used to build the battery model [24], and the diagram for internal resistance model is shown in Figure 2. SOC is the state of charge of the battery, R_{int} is the battery internal resistance, V_{oc} is the open circuit voltage of battery, I_c is the battery current, and U_c is the battery voltage. R_{int} is associated with SOC and I_c. The higher the R_{int}, the lower the battery efficiency for charging. The regenerative braking of the motor is affected by the maximum charging current of the battery. When the SOC of the battery is large, the charging current allowed by the battery is very small. In order to limit the impact of excessive charging current on the battery life, the regenerative braking of the motor cannot be performed when the SOC is large. And the simulations used in this paper do not involve long-term braking process or cycle conditions. Therefore, this paper does not set an additional model to estimate the SOC and take the method to set the SOC to be the initial value. Considering the influences of the battery on the own vehicle, the initial SOC is set to be 0.6.

There are many factors affecting the braking force of the motor. This paper mainly considers the torque-speed characteristic [25]. And the torque-speed characteristic is defined in equation (1), where ω_m is the angular velocity of the motor, ω_0 is the minimum velocity of the motor braking torque, ω_{ini} is the minimum velocity of constant regeneration braking torque, ω_b is the base velocity of the motor, ω_{end} is the maximum speed of motor braking torque, $P_{B\_\max}$ is the maximum braking power of the motor, and $f_m(\omega_m)$ is the correction for the regenerative braking torque according to the motor efficiency. And the diagram for the torque-speed characteristic is shown in Figure 3:

$$T_{M\_\max} = \begin{cases} 0, & \omega_m < \omega_0, \omega_{\text{end}} \le \omega_m, \\ \dfrac{9550 P_{B\_\max}}{\omega_b}, & \omega_{\text{ini}} \le \omega_m \le \omega_b, \\ \dfrac{9550 P_{B\_\max}}{\omega_m} f_m(\omega_m), & \omega_0 \le \omega_m \le \omega_{\text{ini}}, \\ \dfrac{9550 P_{B\_\max}}{\omega_m}, & \omega_b \le \omega_m \le \omega_{\text{end}}. \end{cases} \tag{1}$$

During regenerative braking, the motor can be used as a generator to convert mechanical energy into electrical energy. And the battery pack is charged with the electric energy from the motor. So the efficiency of energy recovery during braking process is related to the efficiencies of charging and motor power generation.

The power generation efficiency η_m of the motor is related to torque T_{reb} and the speed of the motor during the regenerative braking, and it can be defined as

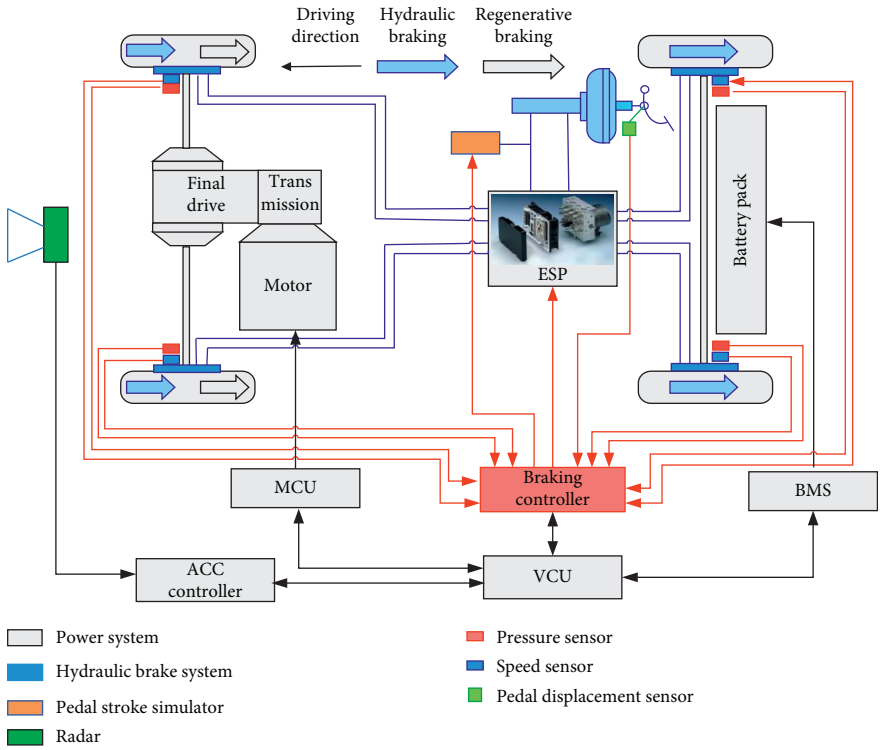

Figure 1: The structural diagram of the BEV with regeneration braking.

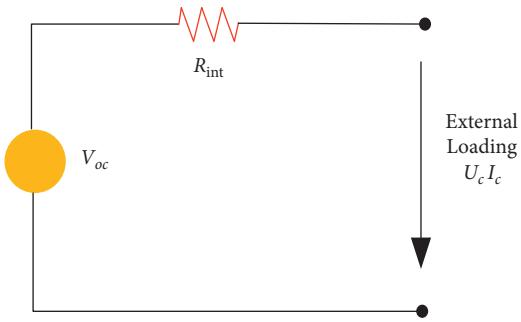

Figure 2: The diagram of the internal resistance model.

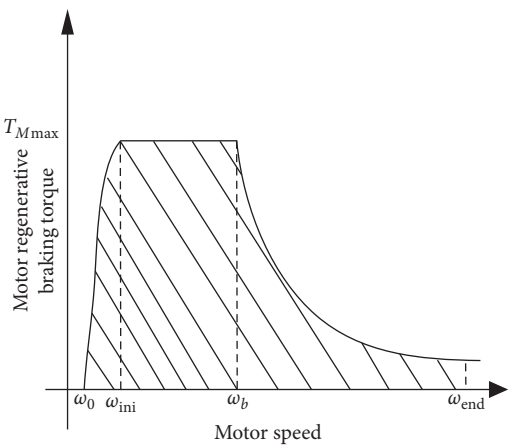

Figure 3: The diagram of the torque-speed characteristic.

$$\eta_m = \frac{U_c I_c}{T_{reb}\omega_m}. \tag{2}$$

The power P_m generated by the motor can be defined as

$$P_m = T_{reb}\omega_m \eta_m (T_{reb}, \omega_m). \tag{3}$$

The charging efficiency of battery η_b is related to the SOC and I_c, and the power for the charging P_{b_chg} can be defined as

$$P_{b\_chg} = I_c U_c \eta_b (I_c, \mathrm{SOC}). \tag{4}$$

Combining equations (2)–(4), the effective power of energy recovery for the battery pack during regenerative braking process can be defined as

$$P_{b\_chg} = T_{reb}\omega_m \eta_m (T_{reb}, \omega_m)\eta_b (I_c, \mathrm{SOC}). \tag{5}$$

The key parameters of the BEV model are presented in Table 1.

3. Hierarchical Control Structure

The ACC system in this paper adopts a hierarchical structure for control and an upper controller and a lower controller form the hierarchical structure [26]. And the upper controller is used as a decision layer, and a lower controller is used as a control layer. The diagram of the hierarchical control structure is shown in Figure 4.

When there is no vehicle in front of the own vehicle, the own vehicle is in speed control mode, and the own vehicle drives at the speed preset by the driver. When there is a vehicle in front of the own vehicle, the own vehicle is in the

Table 1: Main parameters for the BEV model.

Symbol	Description	Values
M_v	Vehicle weight	1550 kg
A	Front area	2.28 m^2
C_w	Drag coefficient	0.36
f_r	Rolling resistance coefficient	0.015
ρ_{air}	Air density	1.206 kg/m^3
P_{M_max}	Maximum power of the motor	87 KW
SOC_{ini}	Initial SOC	0.6
Q_{bat}	Total battery capacity	93 Ah

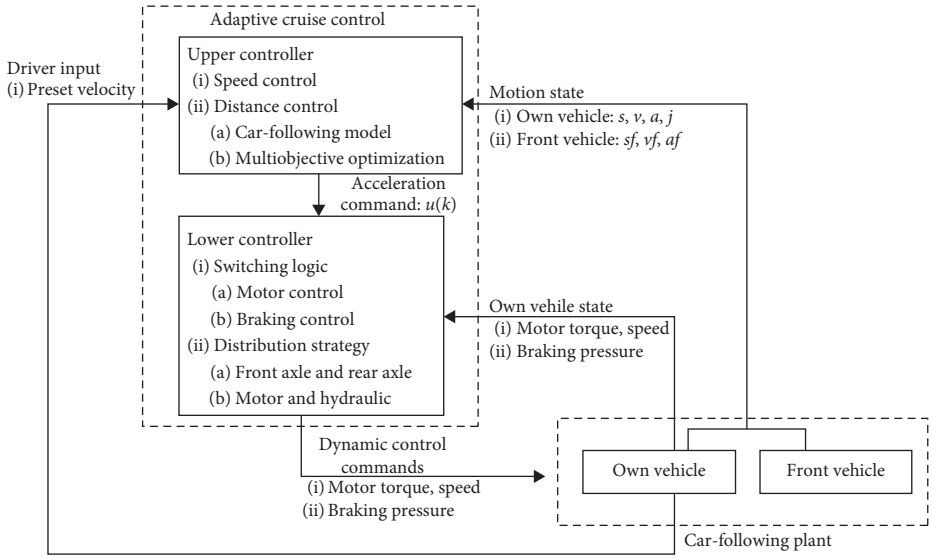

Figure 4: The diagram of the hierarchical control structure of the ACC system.

distance control mode, and the upper controller for the distance control mode contains a longitudinal car-following model and an optimization algorithm for multiple objectives. The upper controller calculates the optimized control command for the acceleration to act on the lower controller according to the motion state of the own vehicle and the front vehicle. The lower controller includes a switching logic, and a distribution strategy for braking force. The switching logic contains a drive control strategy for motor, an ESC-based brake control strategy, and so on. The distribution strategy contains distribution strategy of braking force for front axle and rear axle, and distribution strategy of braking force for motor and hydraulic. The lower controller tracks the control command of acceleration based on the feedback signal of own vehicle state and produces the signals of brake pressure and motor torque and speed to act on the own vehicle.

4. Lower Controller

In the hierarchical structure, the upper controller is applied to calculate the expected acceleration, and the lower controller is used to determine that the own vehicle is in driving mode or braking mode to track the control command. The distribution strategy for braking force is an important component of the lower controller in this paper.

The distribution strategy for braking force is the focus of the energy recovery system, including the braking force distribution for the front axle and rear axle which affects the stability of braking, and the distribution for the motor braking force and hydraulic braking force which affects the energy recovery efficiency [23]. Brake stability and energy recovery efficiency need to be considered in coordination. To maximize the recovery of braking energy, the motor on front axle needs to provide more braking force as much as possible. However, too much braking force on front axle will cause the vehicle to be unstable. Therefore, the distribution strategy for braking force is designed considering the restrictions of the ECE regulations on the braking force of the front axle and rear axle. The distribution strategy of braking force in this paper is shown in Figure 5.

Braking strength z is an important variable in the distribution strategy for braking force, it is the ratio of deceleration a_{dec} to acceleration of gravity g, and it is defined in equation (6). β is the distribution coefficient of braking force and is defined in equation (7):

$$z = \frac{a_{dec}}{g}, \tag{6}$$

$$\beta = \frac{F_{bf}}{F_b} = \frac{F_{bf}}{F_{bf} + F_{br}}. \tag{7}$$

Considering the ECE regulations for braking stability requirements, some constraints should be put on β as follows:

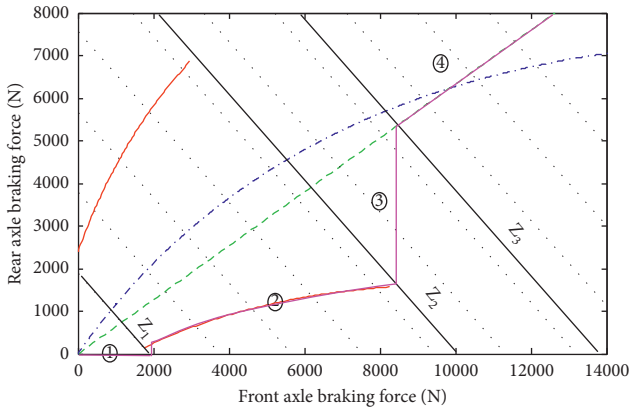

Figure 5: The diagram of braking force distribution strategy.

$$\begin{cases} \beta \geq \dfrac{(b + zh_g)}{L}, & 0.15 \leq z \leq 0.8, \\ \beta \leq \dfrac{(z + 0.04)(b + zh_g)}{0.7zL}, & 0.1 \leq z \leq 0.52, \\ \beta \geq 1 - \dfrac{(z + 0.04)(a - zh_g)}{0.7zL}, & 0.1 \leq z \leq 0.52. \end{cases} \tag{8}$$

The calculation of braking force for the front axle and rear axle is given below, and the descriptions of the parameters involved in the calculation process are shown in Table 2.

When $z < z_1$, a lower limit of the braking force for the front axle is not required in the regulation, braking force is obtained only by motor braking on front axle, and they are defined as

$$\begin{aligned} F_{bf} &= F_b, \\ F_{br} &= 0. \end{aligned} \tag{9}$$

When $z_1 < z < z_2$, braking forces on the front axle and rear axle are distributed along the lower limit for ECE regulations, and they are defined as

$$\begin{cases} F_{bf} = F_b \left(1 - \dfrac{(z + 0.04)(l_1 - zh_g)}{0.7zL}\right), \\ F_{bf} = F_b \dfrac{(z + 0.04)(l_1 - zh_g)}{0.7zL}. \end{cases} \tag{10}$$

When $z_2 < z < z_3$, the braking strength is high, the motor braking achieves its maximum, the braking force for front axle is constant, and the hydraulic braking force for the rear axle is increased, and they are defined as

$$\begin{aligned} F_{bf} &= \frac{T_{B\_\max} \cdot i_r}{r_w}, \\ F_{br} &= F_b - F_{bf}. \end{aligned} \tag{11}$$

Table 2: Parameters in distribution strategy of braking force.

Symbol	Description
F_b	Total demand braking force
F_{bf}	Braking force of front axle
F_{br}	Braking force of rear axle
L	Wheelbase
h_g	Centroid height
l_1	Distance from centroid to front axle
$T_{B\_\max}$	Maximum braking torque of motor
i_r	Transmission ratio of main reducer
r_w	Tire rolling radius

When $z > z_3$, the motor brake is abandoned, and the braking forces on the front axle and rear axle are distributed along the line of braking force distribution to ensure the safety and take advantage of the ground attachment characteristics. And they are defined in equation (12). In the process of braking force distribution, if the motor braking force is insufficient, it is compensated through the hydraulic braking force:

$$\begin{aligned} F_{bf} &= F_b \beta, \\ F_{br} &= F_b (1 - \beta). \end{aligned} \tag{12}$$

5. Upper Controller

5.1. Longitudinal Car-Following Model. To design the upper controller, the car-following model needs to be established firstly. In this paper, the car-following model is based on the longitudinal motion relationship of the front vehicle and the own vehicle.

The spacing Δs and relative velocity v_{rel} at moment k are defined as follows:

$$\Delta s(k) = s_f(k) - s(k), \tag{13}$$

$$v_{\text{rel}}(k) = v_f(k) - v(k), \tag{14}$$

where s_f and s are the distances of the front vehicle and the own vehicle, respectively, and v_f and v are the speeds of the front vehicle and the own vehicle, respectively.

At moment $k + 1$, the distance of the front vehicle and the own vehicle is defined as follows:

$$s_f(k+1) = s_f(k) + v_f(k)T_s + \frac{1}{2}a_f(k)T_s^2, \tag{15}$$

$$s(k+1) = s(k) + v(k)T_s + \frac{1}{2}a(k)T_s^2, \tag{16}$$

where a_f and a are the acceleration of the front vehicle and the own vehicle, respectively, and T_s is the sampling time.

At moment $k + 1$, the velocity of the front vehicle and the own vehicle is defined as follows:

$$v_f(k+1) = v_f(k) + a_f(k)T_s, \tag{17}$$

$$v(k+1) = v(k) + a(k)T_s. \tag{18}$$

At moment $k+1$, the spacing and relative velocity are defined as follows:

$$\Delta s(k+1) = s_f(k+1) - s(k+1), \tag{19}$$

$$v_{\text{rel}}(k+1) = v_f(k+1) - s(k+1). \tag{20}$$

Combining equations (13)–(16) and (19), the following equation can be obtained:

$$\Delta s(k+1) = \Delta s(k) + v_{\text{rel}}(k)T_s + \frac{1}{2}a_f(k)T_s^2 - \frac{1}{2}a(k)T_s^2. \tag{21}$$

Combining equations (14), (17), (18), and (20), the following equation can be obtained:

$$v_{\text{rel}}(k+1) = v_{\text{rel}}(k) + a_f(k)T_s - a(k)T_s. \tag{22}$$

When the upper controller for the ACC system is designed, due to the foundation of the lower controller, it can be considered that the actual acceleration of the own vehicle a and control command for acceleration (also called expected acceleration) u satisfy the following relationship [13, 26]:

$$a(k+1) = \left(1 - \frac{T_s}{\tau}\right)a(k) + \frac{T_s}{\tau}u(k), \tag{23}$$

where u is the control command for acceleration and τ is the time constant of the lower controller.

The rate of change of acceleration is also called jerk, and the jerk at moment k can be defined as follows:

$$j(k) = \frac{a(k) - a(k-1)}{T_s}. \tag{24}$$

At moment $k+1$, the jerk can be defined as follows:

$$j(k+1) = \frac{a(k+1) - a(k)}{T_s}. \tag{25}$$

Combining equations (23) and (25), the following equation can be obtained:

$$j(k+1) = -\frac{1}{\tau}a(k) + \frac{1}{\tau}u(k). \tag{26}$$

The spacing, speed of the own vehicle, relative velocity, acceleration of the own vehicle, and jerk for the own vehicle are selected as the state vector, and they are defined as

$$x(k) = \left[\Delta s(k), v(k), v_{\text{rel}}(k), a(k), j(k)\right]^T. \tag{27}$$

The acceleration for the front vehicle is selected as the disturbance, and it is defined as

$$w(k) = a_f(k). \tag{28}$$

Combining equations (18), (21)–(23), and (26), the car-following model in the longitudinal direction is defined:

$$x(k+1) = Ax(k) + Bu(k) + Gw(k), \tag{29}$$

where

$$A = \begin{bmatrix} 1 & 0 & T_s & -\frac{1}{2}T_s^2 & 0 \\ 0 & 1 & 0 & T_s & 0 \\ 0 & 0 & 1 & -T_s & 0 \\ 0 & 0 & 0 & 1 - \frac{T_s}{\tau} & 0 \\ 0 & 0 & 0 & -\frac{1}{\tau} & 0 \end{bmatrix},$$

$$B = \begin{bmatrix} 0 \\ 0 \\ 0 \\ \frac{T_s}{\tau} \\ \frac{1}{\tau} \end{bmatrix}, \tag{30}$$

$$G = \begin{bmatrix} \frac{1}{2}T_s^2 \\ 0 \\ T_s \\ 0 \\ 0 \end{bmatrix}.$$

5.2. Model Predictive Control (MPC) for Multiple Objectives. In the multiobjective-optimized upper controller, the control objectives enable the own vehicle to guarantee safety, tracking, comfort, and energy economy in the driving process. To achieve these control objectives, the multiple objectives are analyzed based on the car-following model. The multiple objectives are transformed into the corresponding system constraints and performance indicators. And the optimization for multiple objectives in the driving process is finally transformed into a constrained optimization proposition.

Δs_{des} is the expected spacing obtained from the constant time headway (CTH) spacing policy, δ is the difference between the real spacing and the expected spacing, and Δs_{des} and δ at moment k can be defined:

$$\Delta s_{\text{des}}(k) = d_0 + t_h \cdot v(k), \tag{31}$$

$$\delta(k) = \Delta s(k) - \Delta s_{\text{des}}(k), \tag{32}$$

where d_0 is the fixed distance between the two vehicles when the vehicle speed is low and zero and t_h is the time headway.

To ensure the tracking in the car-following process, the actual spacing between the two vehicles approaches the expected spacing calculated by the spacing strategy, and the velocity of the own vehicle should be close to the velocity of the front vehicle; that is, the two vehicles are in a relatively static state [26]:

$$\text{objectives}: \begin{cases} \delta(k) \longrightarrow 0, & \text{as } k \longrightarrow \infty, \\ v_{\text{rel}}(k) \longrightarrow 0, & \text{as } k \longrightarrow \infty. \end{cases} \tag{33}$$

To improve the comfort during the car-following process, the range of fluctuation for acceleration and jerk should be minimized:

$$\text{objectives}: \begin{cases} \min |a(k)|, \\ \min |j(k)|. \end{cases} \tag{34}$$

From above analysis, the spacing error, relative velocity, acceleration of the own vehicle, and jerk of the own vehicle are chosen as the performance vector, and the performance vector is defined:

$$y(k) = [\delta(k), v_{\text{rel}}(k), a(k), j(k)]^T. \tag{35}$$

The following relationship can be established between the performance vector and the state variable:

$$y(k) = Cx(k) - Z, \tag{36}$$

where

$$C = \begin{bmatrix} 1 & -t_h & 0 & 0 & 0 \\ 0 & 0 & 1 & 0 & 0 \\ 0 & 0 & 0 & 1 & 0 \\ 0 & 0 & 0 & 0 & 1 \end{bmatrix}, \quad Z = \begin{bmatrix} d_0 \\ 0 \\ 0 \\ 0 \end{bmatrix}. \tag{37}$$

During the car-following process, a smooth system response is preferred. To smooth the response, the exponential decay function is introduced to be reference trajectory of performance vector.

The coefficient of the error of spacing in reference trajectory is defined in the following equation, and other coefficients can be defined in a similar way:

$$\begin{aligned} \delta_r(k+i) &= \delta(k) + [\delta_{\text{des}}(k) - \delta(k)]\left[1 - e^{(-iT_s/\alpha_\delta)}\right] \\ &= \delta(k) + [0 - \delta(k)]\left[1 - e^{(-iT_s/\alpha_\delta)}\right] \\ &= \rho_\delta^i \delta(k), \\ \rho_\delta &= e^{(-T_s/\alpha_\delta)}, \quad 0 < \rho_\delta < 1, \end{aligned} \tag{38}$$

where δ_r is the reference trajectory for the error of spacing and α is the time constant of the reference trajectory for the error of spacing.

The system response is smoothed as follows:

$$y_r(k+i) = \begin{bmatrix} \rho_\delta^i & & & \\ & \rho_{v_{\text{rel}}}^i & & \\ & & \rho_a^i & \\ & & & \rho_j^i \end{bmatrix} y(k), \tag{39}$$

where ρ_δ, $\rho_{v_{\text{rel}}}$, ρ_a, and ρ_j are the coefficients in reference trajectory, ρ_δ is the coefficient of the spacing error, $\rho_{v_{\text{rel}}}$ is the coefficient of relative velocity, ρ_a is the coefficient of the acceleration of the own vehicle, and ρ_j is the coefficient of the jerk of the own vehicle.

The values of these coefficients are between 0 and 1. Along the reference trajectory, the performance vector approaches zero smoothly, rather than approaching zero directly.

As for the energy economy, it is related to the acceleration. And the acceleration is determined by the control command of acceleration. Therefore, the control command of acceleration is selected as the performance index of the energy economy [27]. To improve the energy economy, the absolute value of control command should be minimized:

$$\text{objective}: \min |u(k)|. \tag{40}$$

No matter what control algorithm is used, the safety is the primary objective of an ACC system. Although we can guarantee a safe expected spacing through the spacing strategy, the collision is likely to happen before reaching the expected spacing. Therefore, for the purpose of ensuring the safety of two vehicles throughout the driving process, the actual vehicle spacing must be constrained as follows:

$$\Delta s(k) = s_p(k) - s(k) \geq d_c, \tag{41}$$

where d_c is the minimum safe spacing between two vehicles.

Taking into account the limitations of the vehicles own capacity, it needs to constrain the velocity, acceleration, jerk, and acceleration command for the own vehicle. The constraints can be defined:

$$\begin{cases} v_{\min} \leq v(k) \leq v_{\max}, \\ a_{\min} \leq a(k) \leq a_{\max}, \\ j_{\min} \leq j(k) \leq j_{\max}, \\ u_{\min} \leq u(k) \leq u_{\max}. \end{cases} \tag{42}$$

Because of the advantages of MPC in achieving multiobjective optimization [27–29], the MPC is applied into the multiobjective optimization of the ACC system.

Predictive form for the state vector and performance vector are defined as follows:

$$\hat{X}_p(k+p \mid k) = \overline{A}x(k) + \overline{B}U(k+m) + \overline{G}W(k+p), \tag{43}$$

$$\hat{Y}_p(k+p \mid k) = \overline{C}x(k) + \overline{D}U(k+m) + \overline{E}W(k+p) - \overline{Z}, \tag{44}$$

where

$$\hat{X}_p(k+p\,|\,k)=\begin{bmatrix}\hat{x}_p(k+1\,|\,k)\\ \hat{x}_p(k+2\,|\,k)\\ \vdots\\ \hat{x}_p(k+p\,|\,k)\end{bmatrix},$$

$$\hat{Y}_p(k+p\,|\,k)=\begin{bmatrix}\hat{y}_p(k+1\,|\,k)\\ \hat{y}_p(k+2\,|\,k)\\ \vdots\\ \hat{y}_p(k+p\,|\,k)\end{bmatrix},$$

$$U(k+m)=\begin{bmatrix}u(k)\\ u(k+1)\\ \vdots\\ u(k+m-1)\end{bmatrix},$$

$$W(k+p)=\begin{bmatrix}w(k)\\ w(k+1)\\ \vdots\\ w(k+p-1)\end{bmatrix},$$

$$\overline{A}=\begin{bmatrix}A\\ A^2\\ \vdots\\ A^p\end{bmatrix},$$

$$\overline{B}=\begin{bmatrix}B & 0 & \cdots & 0\\ AB & B & \ddots & 0\\ \vdots & \vdots & \ddots & \vdots\\ A^{p-1}B & A^{p-2}B & \cdots & A^{p-m}B\end{bmatrix},\tag{45}$$

$$\overline{G}=\begin{bmatrix}G & 0 & \cdots & 0\\ AG & G & \ddots & \vdots\\ \vdots & \vdots & \ddots & 0\\ A^{p-1}G & A^{p-2}G & \cdots & G\end{bmatrix},$$

$$\overline{C}=\begin{bmatrix}CA\\ CA^2\\ \vdots\\ CA^p\end{bmatrix},$$

$$\overline{D}=\begin{bmatrix}CB & 0 & \cdots & 0\\ CAB & CB & \ddots & 0\\ \vdots & \vdots & \ddots & \vdots\\ CA^{p-1}B & CA^{p-2}B & \cdots & CA^{p-m}B\end{bmatrix},$$

$$\overline{E}=\begin{bmatrix}CG & 0 & \cdots & 0\\ CAG & CG & \ddots & \vdots\\ \vdots & \vdots & \ddots & 0\\ CA^{p-1}G & CA^{p-2}G & \cdots & CG\end{bmatrix},$$

$$\overline{Z}=\begin{bmatrix}Z\\ Z\\ \vdots\\ Z\end{bmatrix}.$$

where $x_p(k+i\,|\,k)$ is the predictive value of the state vector for $k+i$ moment at the moment k, $y_p(k+i\,|\,k)$ is the predictive value of the performance vector for $k+i$ moment at the moment k, $U(k+m)$ is the matrix for the sequence of the control command, p is the predictive horizon, and m is the control horizon.

And considering the different objectives in equations (33), (34), and (40) and the reference trajectory in equation (39), the discretized objective function based on MPC can be obtained:

$$J=\sum_{i=1}^{p}\left[y_p(k+i\,|\,k)-y_r(k+i)\right]^T Q\left[y_p(k+i\,|\,k)-y_r(k+i)\right]+\sum_{j=0}^{m-1}u(k+j)^T Ru(k+j),\tag{46}$$

where Q and R are the weight matrices and $u(k+i)$ is the control command at moment $k+i$.

Combining the equations (44) and (46), the following equation can be obtained:

$$J=V^T\overline{Q}V+U(k+m)^T\overline{R}U(k+m),\tag{47}$$

where

$$V=\overline{C}x(k)+\overline{D}U(k+m)+\overline{E}W(k+p)-\overline{Z}-\overline{\Phi}Cx(k)+\overline{\Phi}Z,$$

$$\overline{Q}=\begin{bmatrix}Q & \cdots & 0\\ \vdots & \ddots & \vdots\\ 0 & \cdots & Q\end{bmatrix},$$

$$\overline{R}=\begin{bmatrix}R & \cdots & 0\\ \vdots & \ddots & \vdots\\ 0 & \cdots & R\end{bmatrix},$$

$$\overline{\Phi}=\begin{bmatrix}\Psi_1\\ \Psi_2\\ \vdots\\ \Psi_p\end{bmatrix},$$

$$\Psi_i=\begin{bmatrix}\rho_\delta^i & 0 & 0 & 0\\ 0 & \rho_{v_{\text{rel}}}^i & 0 & 0\\ 0 & 0 & \rho_a^i & 0\\ 0 & 0 & 0 & \rho_j^i\end{bmatrix}.\tag{48}$$

Expand equation (47) to retain the items related to $U(k+m)$, the following equation can be obtained:

$$J=U(k+m)^T\left(\overline{R}+\overline{D}^T\overline{Q}\overline{D}\right)U(k+m)+2\left\{x(k)^T\left[\overline{C}^T-\overline{C}^T\overline{\Phi}^T\right]\overline{Q}\overline{D}+W(k+p)^T\overline{E}^T\overline{Q}\overline{D}-\left(\overline{Z}^T-\overline{Z}^T\overline{\Phi}^T\right)\overline{Q}\overline{D}\right\}U(k+m).\tag{49}$$

All the constraints in this paper can be summarized in the following form:

$$\begin{cases} \Delta x(k) \geq d_c, \\ v_{\min} \leq v(k) \leq v_{\max}, \\ a_{\min} \leq a(k) \leq a_{\max}, \\ j_{\min} \leq j(k) \leq j_{\max}, \\ u_{\min} \leq u(k) \leq u_{\max}. \end{cases} \tag{50}$$

Convert equation (50) into the form of matrix inequality, the following equation can be obtained:

$$\begin{cases} \overline{M} \leq \overline{L}\hat{X}_p(k+p) \leq \overline{N}, \\ U(k+m) \leq U_{\max}, \\ -U(k+m) \leq -U_{\min}, \end{cases} \tag{51}$$

where

$$M = \begin{bmatrix} d_c \\ v_{\min} \\ a_{\min} \\ j_{\min} \end{bmatrix},$$

$$N = \begin{bmatrix} Inf \\ v_{\max} \\ a_{\max} \\ j_{\max} \end{bmatrix},$$

$$L = \begin{bmatrix} 1 & 0 & 0 & 0 & 0 \\ 0 & 1 & 0 & 0 & 0 \\ 0 & 0 & 0 & 1 & 0 \\ 0 & 0 & 0 & 0 & 1 \end{bmatrix},$$

$$\overline{L} = \begin{bmatrix} L & 0 & 0 & \cdots & 0 & 0 \\ 0 & L & 0 & 0 & \cdots & 0 \\ 0 & 0 & \ddots & 0 & \cdots & 0 \\ 0 & \cdots & 0 & \ddots & 0 & 0 \\ 0 & 0 & \cdots & 0 & L & 0 \\ 0 & 0 & \cdots & 0 & 0 & L \end{bmatrix}_{p \times p}, \tag{52}$$

$$\overline{M} = \begin{bmatrix} M \\ M \\ \vdots \\ M \end{bmatrix},$$

$$\overline{N} = \begin{bmatrix} N \\ N \\ \vdots \\ N \end{bmatrix},$$

$$U_{\max} = \begin{bmatrix} u_{\max} \\ \vdots \\ u_{\max} \end{bmatrix},$$

$$U_{\min} = \begin{bmatrix} u_{\min} \\ \vdots \\ u_{\min} \end{bmatrix}.$$

Combining equations (43) and (51), the following equation for constraints can be obtained:

$$\Omega U(k+m) \leq T, \tag{53}$$

where

$$\Omega = \begin{bmatrix} \overline{L}\overline{B} & -\overline{L}\overline{B} & I & -I \end{bmatrix}^T,$$

$$T = \begin{bmatrix} \overline{N} - \overline{L}\overline{G}W(k+p) - \overline{L}\overline{A}x(k) \\ -\overline{M} + \overline{L}\overline{G}W(k+p) + \overline{L}\overline{A}x(k) \\ U_{\max} \\ -U_{\min} \end{bmatrix}. \tag{54}$$

The objective function in equation (49) combined with the constraints in equations (53) can be converted to an optimization problem in the following equation that can be solved by quadratic programming [30, 31]:

$$\begin{aligned} \min \quad & \left\{ U(k+m)^T K U(k+m) + 2SU(k+m) \right\} \\ \text{s.t.} \quad & \Omega U(k+m) \leq T, \end{aligned} \tag{55}$$

where

$$\begin{aligned} K &= \overline{R} + \overline{D}^T \overline{Q} \overline{D}, \\ S &= x(k)^T \left[\overline{C}^T - \overline{C}^T \overline{\Phi}^T \right] \overline{Q}\overline{D} + W(k+p)^T \overline{E}^T \overline{Q}\overline{D} \\ &\quad - \left(\overline{Z}^T - \overline{Z}^T \overline{\Phi}^T \right) \overline{Q}\overline{D}. \end{aligned} \tag{56}$$

Optimal control variable $U^*(k+m)$ can be solved from the quadratic programming problem in equation (55). And only the first component of $U^*(k+m)$ can be applied to the ACC system as the optimal acceleration command. And at the next moment, the above process is repeated. This reflects the receding horizon optimization in MPC.

6. Methods

To evaluate the performances of the proposed ACC strategy, two different strategies are compared. The control strategy studied in this paper contains comfort, energy economy, safety, and tracking. And the strategy that contains safety and tracking is the contrast strategy. In the contrast control strategy, the braking energy recovery is not considered in the lower controller or the BEV model, the coefficients for R is zero, the optimized reference trajectories are not applied to the objective function, and there are no strict constraints on jerk. The abbreviations for the proposed control strategy and contrast control strategy are BER_CEST and NO_ST, respectively.

The minimum safe spacing is an important indicator for the safety, and when the spacing is bigger than it, the driving process is considered safe. The capability of adjusting the difference of spacing to zero and the capability of regulating the relative velocity to zero are regarded as the measurement of the tracking. The maximum value of jerk's absolute value is an important indicator for the comfort during the driving process, and the limit of the indicator for comfort is 3 m/s^3. Energy economy is estimated by the change of SOC. The

strategies are designed with the Matlab/Simulink, and the simulation experiment is performed combined with the Carsim platform.

Scenario in simulation is set as follows: (1) The speed of the front vehicle is changing and (2) cut in. These two scenarios are representative scenarios. Wherein, conventional driving process for the two vehicles is shown in scenario 1, and the urgent driving process for the two vehicles is shown in scenario 2. Settings for two simulation scenarios are shown in Table 3, where $\Delta s_$ini is the initial vehicle spacing, $v_$ini and $v_f_$ini are the initial speed for the own vehicle and the front vehicle, respectively, and $a_$amp is the amplitude of acceleration for the front vehicle. The main parameters for the multiobjective optimization algorithm are listed in Table 4.

Table 3: Settings for two simulation scenarios.

Scenario	$\Delta s_$ini (m)	$v_$ini (m/s)	$v_f_$ini (m/s)	$a_$amp (m/s^2)
1	50	10	15	2
2	30	15	10	2

Table 4: Parameters in the simulation process.

Symbol	Values
T_s	0.2 s
τ	0.15 s
d_0	7 m
d_c	5 m
$v_{\min}$	0 m/s
$v_{\max}$	36 m/s
$a_{\min}$	−5.5 m/s^2
$a_{\max}$	2.5 m/s^2
$u_{\min}$	−5.5 m/s^2
$u_{\max}$	2.5 m/s^2
$j_{\min}$	−3 m/s^3
$j_{\max}$	3 m/s^3
$\rho_\delta, \rho_{v_{\text{rel}}}, \rho_a, \rho_j$	0.94
Q	diag{1, 10, 1, 1}
R	1
p	10
m	5

7. Simulation Experiment and Discussion

7.1. Scenario 1. In real life, following a front vehicle with a variable speed is a familiar traffic scenario. This scenario mainly examines the capability of speed adjustment and tracking for the own vehicle when the speed of the front vehicle changes on a single lane. The simulation results in scenario 1 are shown in Figure 6. From Figure 6(a), it can be seen that the vehicle spacing is greater than minimum safe spacing in two control strategies, so the safety is ensured in both control strategies. From Figures 6(a) and 6(b), the tracking can be ensured in both control strategies. For the desired spacing, the tracking ability is better in NO_ST, and for the speed of the front vehicle, the tracking ability is better in BER_CEST. This is a compromise among various control objectives in BER_CEST.

From Figure 6(c), the fluctuation range for acceleration is bigger in NO_ST than BER_CEST, while the curve of the acceleration in BER_CEST is relatively smooth. From Figure 6(d), the maximum value of the jerk's absolute value in NO_ST is 18.66 m/s^3, which exceeds 3 m/s^3. However, the maximum value of the jerk's absolute value in BER_CEST is always within the 3 m/s^3. Therefore, the comfort in BER_CEST is improved compared with the NO_ST. The reasons for this are that the jerk is strictly constrained, and the optimized reference trajectory are applied to improve the comfort in BER_CEST. Driving is more stable while comfort is improved. Therefore, the driving stability is also improved because of the introduction of the optimized reference trajectory and the application of the strict constraints on jerk. From Figure 6(e), it is shown that the battery power in BER_CEST changes between positive and negative. However, the battery power in NO_ST changes between zero and positive. This is because the energy is recovered during braking process in BER_CEST. From Figure 6(f), the change of SOC for two strategies is 0.0020 and 0.0042, respectively. The improvement of the energy economy for BER_CEST is 52.03% compared with NO_ST. The reasons for this are that the energy consumption is optimized in the upper controller and the braking energy recovery is considered in the lower controller in BER_CEST. Therefore, the energy economy is improved in BER_CEST.

From the above analysis, BER_CEST adopts the optimized reference trajectory and strict constraints on jerk to improve the comfort, and the energy economy is considered both in the upper controller and the lower controller. So BER_CEST can obtain better comfort and energy economy compared with NO_ST based on ensuring the safety and tracking.

7.2. Scenario 2. In the cut in scenario, in the driving process of the own vehicle, the front vehicle of the adjacent lane suddenly changes lane, and the front vehicle is inserted in front of the own vehicle. The simulation results of scenario 2 are shown in Figure 7. From Figure 7(a), because the spacing between two vehicles is bigger than 5 m, the driving processes both are safe in two control strategies. From Figures 7(a) and 7(b), the own vehicle can track the desired vehicle spacing and the velocity of front vehicle in two strategies. For the desired spacing, the tracking ability is better in NO_ST, and for the speed of the front vehicle, the tracking abilities are closer in both strategies. This is a compromise among various control objectives in BER_CEST.

From Figure 7(c), the fluctuation range for the acceleration is bigger in NO_ST, while the curve of acceleration is relatively smooth in BER_CEST. From Figure 7(d), the maximum value of the jerk's absolute value in NO_ST is 16.49 m/s^3, which exceeds 3 m/s^3. But, the maximum value of the jerk's absolute value in BER_CEST is always within 3 m/s^3. The comfort in BER_CEST is improved compared with NO_ST. The reasons for this are that the jerk is strictly constrained, and the optimized reference trajectory is applied to improve the comfort. Driving is more stable while comfort is improved. Therefore, the driving stability is also improved because of the introduction of the optimized

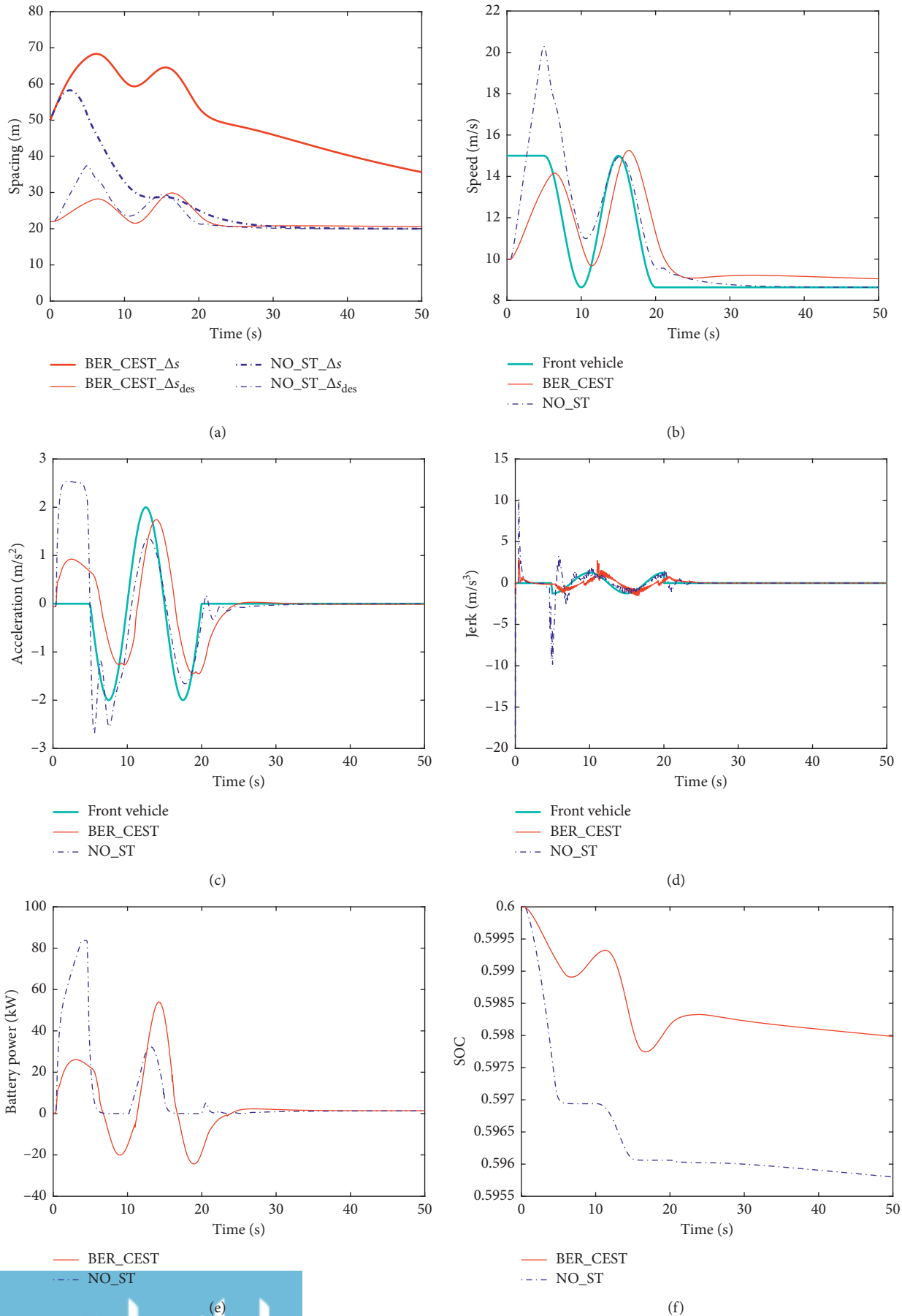

Figure 6: Simulation results of scenario 1. (a) Spacing response. (b) Speed response. (c) Acceleration response. (d) Jerk response. (e) Battery power. (f) SOC.

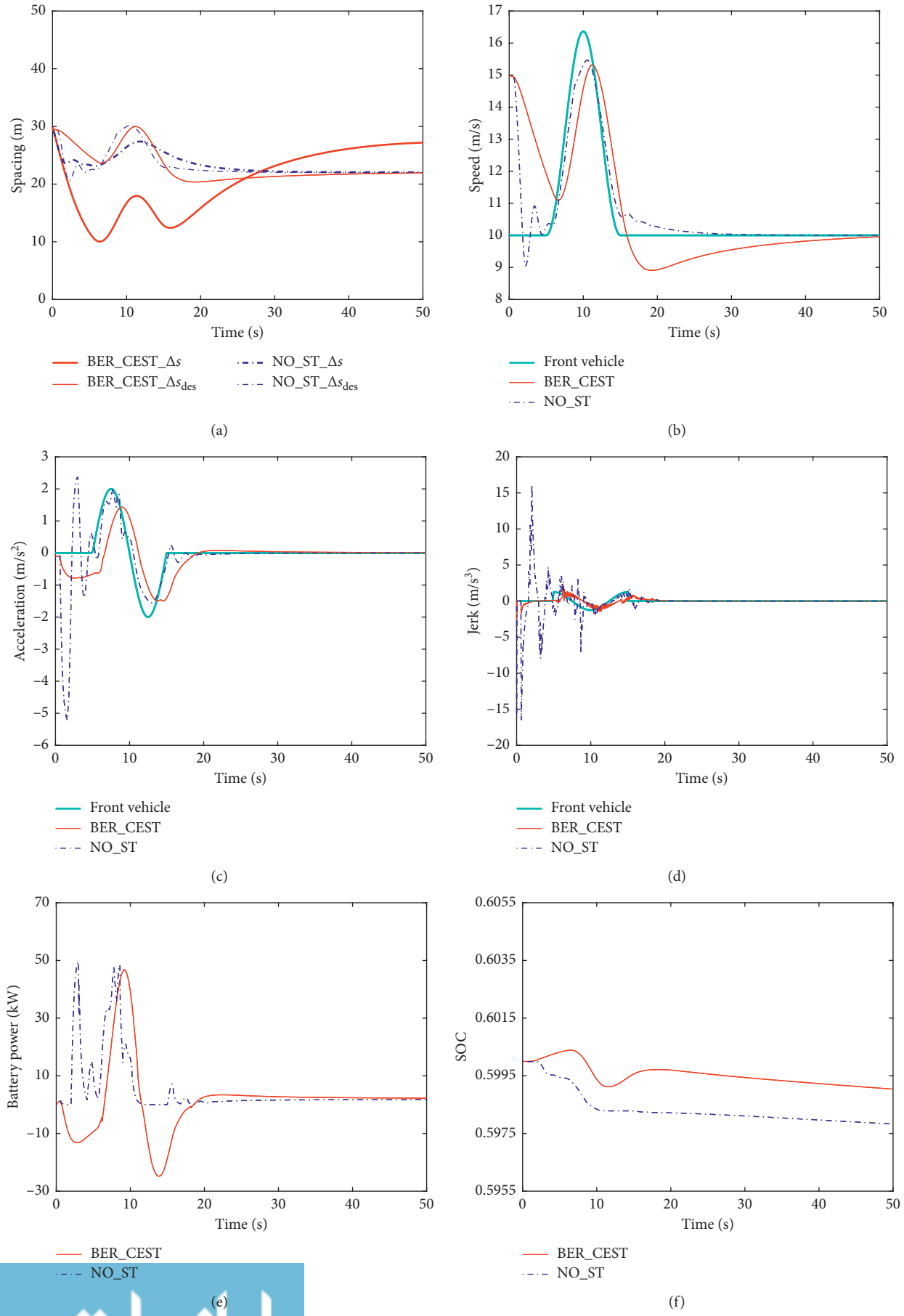

Figure 7: Simulation results of scenario 2. (a) Spacing response. (b) Speed response. (c) Acceleration response. (d) Jerk response. (e) Battery power. (f) SOC.

reference trajectory and the application of the strict constraints on jerk. From Figure 7(e), it is shown that the battery power in BER_CEST changes between positive and negative. However, the battery power in NO_ST changes between zero and positive. This is because the braking energy recovery is considered in the lower controller. From Figure 7(f), the change of SOC for two strategies is 0.00096 and 0.0022, respectively. The improvement of the energy economy for BER_CEST is 55.73% compared with NO_ST. After the front vehicle performs the cut in, the braking energy is recovered during braking process, and the SOC is bigger than the initial SOC. This is because the kinetic energy of BEV is recovered through the regenerative braking during the braking process in BER_CEST.

In summary, BER_CEST adopts the optimized reference trajectories and strict constraints on jerk to improve the comfort, and the energy economy is considered both in the upper controller and the lower controller. So BER_CEST can obtain better comfort and energy economy compared with NO_ST based on ensuring the safety and tracking.

8. Conclusion

In this paper, a hierarchical control architecture is adopted for the proposed ACC strategy on BEV, and the highlight of this paper is that the braking energy recovery is considered in the car-following process. In the proposed control strategy, the safety, tracking, and comfort are considered in the upper controller, and the energy economy is considered both in the upper controller and lower controller. Some conclusions can be obtained as follows: in the upper controller, the acceleration command is optimized in the objective function of MPC to reduce the energy consumption. In the lower controller, the braking energy is recovered during the braking process. So the energy economy is improved. The proposed ACC strategy can improve the comfort for passengers and improve the energy economy for the car owner, so it can promote the wide application of ACC in BEV.

Data Availability

The data used to support the findings of this study are included within the article.

Conflicts of Interest

The authors declare that they have no conflicts of interest.

Acknowledgments

This work was supported by the Basic Research Project of the Knowledge Innovation Program in Shenzhen City (Grant no. JCYJ20170818144449801).

References

[1] Q. P. Liu and C. P. Tang, "Environmental impact assessment of magnesium alloy automobile hub based on life cycle assessment," *Journal of Central South University*, vol. 25, no. 8, pp. 1870–1878, 2018.

[2] Y. Luo, T. Chen, and K. Li, "Multi-objective decoupling algorithm for active distance control of intelligent hybrid electric vehicle," *Mechanical Systems and Signal Processing*, vol. 64-65, pp. 29–45, 2015.

[3] Y. Chen and J. Wang, "Design and evaluation on electric differentials for over-actuated electric ground vehicles with four independent in-wheel motors," *IEEE Transactions on Vehicular Technology*, vol. 61, no. 4, pp. 1534–1542, 2012.

[4] Y. Luo, T. Chen, S. Zhang, and K. Li, "Intelligent hybrid electric vehicle ACC with coordinated control of tracking ability, fuel Economy, and ride comfort," *IEEE Transactions on Intelligent Transportation Systems*, vol. 16, no. 4, pp. 2303–2308, 2015.

[5] L. H. Yang, X. Q. Zhang, J. K. Zhang, and J. T. Liu, "The research of car-following model based on real-time maximum deceleration," *Mathematical Problems in Engineering*, vol. 2015, Article ID 642021, 9 pages, 2015.

[6] X. Ding, H. Guo, R. Xiong, F. Chen, D. Zhang, and C. Gerada, "A new strategy of efficiency enhancement for traction systems in electric vehicles," *Applied Energy*, vol. 205, pp. 880–891, 2017.

[7] R. Xiong, Q. Yu, L. Y. Wang, and C. Lin, "A novel method to obtain the open circuit voltage for the state of charge of lithium ion batteries in electric vehicles by using H infinity filter," *Applied Energy*, vol. 207, pp. 346–353, 2017.

[8] A. K. Madhusudhanan, "A method to improve an electric vehicles range: efficient Cruise Control," *European Journal of Control*, vol. 48, pp. 83–96, 2019.

[9] B. Ganji, A. Z. Kouzani, S. Y. Khoo, and M. Shans-Zahraei, "Adaptive cruise control of a HEV using sliding mode control," *Expert Systems with Applications*, vol. 41, no. 2, pp. 607–615, 2014.

[10] R. Abdullah, A. Hussain, K. Warwick, and A. Zayed, "Autonomous intelligent cruise control using a novel multiple-controller framework incorporating fuzzy-logic-based switching and tuning," *Neurocomputing*, vol. 71, no. 13–15, pp. 2727–2741, 2008.

[11] C. Desjardins and B. Chaib-draa, "Cooperative adaptive cruise control: a reinforcement learning approach," *IEEE Transactions on Intelligent Transportation Systems*, vol. 12, no. 4, pp. 1248–1260, 2011.

[12] A. Weibmann, D. Gorges, and X. H. Lin, "Energy-optimal adaptive cruise control combining model predictive control and dynamic programming," *Control Engineering Practice*, vol. 72, pp. 125–137, 2018.

[13] V. L. Bageshwar, W. L. Garrard, and R. Rajamani, "Model predictive control of transitional maneuvers for adaptive cruise control vehicles," *IEEE Transactions on Vehicular Technology*, vol. 53, no. 5, pp. 1573–1585, 2004.

[14] C. M. Filho, M. H. Terra, and D. F. Wolf, "Safe optimization of highway traffic with robust model predictive control-based cooperative adaptive cruise control," *IEEE Transactions on Intelligent Transportation Systems*, vol. 18, no. 11, pp. 3193–3203, 2017.

[15] M. M. Brugnolli, B. A. Angelico, and A. A. M. Lagana, "Predictive adaptive cruise control using a customized ECU," *IEEE Access*, vol. 7, pp. 55305–55317, 2019.

[16] B. Sakhdari and N. L. Azad, "Adaptive tube-based nonlinear MPC for economic autonomous cruise control of plug-in hybrid electric vehicles," *IEEE Transactions on Vehicular Technology*, vol. 67, no. 12, pp. 11390–11401, 2018.

[17] S. Zhang, Y. Luo, K. Li, and V. Li, "Real-time energy-efficient control for fully electric vehicles based on an explicit model predictive control method," *IEEE Transactions on Vehicular Technology*, vol. 67, no. 6, pp. 4693–4701, 2018.

[18] T. Schwickart, H. Voos, J.-R. Hadji-Minaglou, and M. Darouach, "A fast model-predictive speed controller for minimised charge consumption of electric vehicles," *Asian Journal of Control*, vol. 18, no. 1, pp. 133–149, 2016.

[19] Y. Chen, X. D. Li, C. Wiet, and J. M. Wang, "Energy management and driving strategy for in-wheel motor electric ground vehicles with terrain profile preview," *IEEE Transactions on Industrial Informatics*, vol. 10, no. 3, pp. 1938–1947, 2014.

[20] T. K. Bera, K. Bhattacharya, and A. K. Samantarary, "Bond graph model-based evaluation of a sliding mode controller for a combined regenerative and antilock braking system," *Proceedings of the Institution of Mechanical Engineers, Part I: Journal of Systems and Control Engineering*, vol. 225, no. 17, pp. 918–934, 2011.

[21] D. H. Kim, J. M. Kim, and S. H. Hwang, "Optimal brake torque distribution for a four-wheeldrive hybrid electric vehicle stability enhancement," *Proceedings of the Institution of Mechanical Engineers, Part I: Journal of Systems and Control Engineering*, vol. 221, no. 11, pp. 1357–1366, 2007.

[22] J. M. Zhang, B. Y. Song, and S. M. Cui, "Fuzzy logic approach to regenerative braking system," in *Proceedings of the International Conference on Intelligent Human-Machine Systems and Cybernetics*, pp. 451–454, Hangzhou, China, 2009.

[23] G. Xu, W. Li, K. Xu, and Z. Song, "An intelligent regenerative braking strategy for electric vehicles," *Energies*, vol. 4, no. 9, pp. 1461–1477, 2011.

[24] A. Abdollahi, X. Han, G. V. Avvari et al., "Optimal battery charging, part I: minimizing time-to-charge, energy loss, and temperature rise for OCV-resistance battery model," *Journal of Power Sources*, vol. 303, pp. 388–398, 2016.

[25] L. Li, Y. Zhang, C. Yang, B. Yan, and C. Marina Martinez, "Model predictive control-based efficient energy recovery control strategy for regenerative braking system of hybrid electric bus," *Energy Conversion and Management*, vol. 111, pp. 299–314, 2016.

[26] S. Li, K. Li, R. Rajamani, and J. Wang, "Model predictive multi-objective vehicular adaptive cruise control," *IEEE Transactions on Control Systems Technology*, vol. 19, no. 3, pp. 556–566, 2011.

[27] R. N. Dang, H. Chaoche, Q. Zhang, K. Q. Li, and Y. S. Li, "ACC of electric vehicles with coordination control of fuel economy and tracking safety," in *Proceedings of the 2012 IEEE Intelligent Vehicles Symposium*, pp. 240–245, Alcala de Henares, Spain, June 2012.

[28] C. Zhai, Y. Liu, and F. Luo, "A switched control strategy of heterogeneous vehicle platoon for multiple objectives with state constraints," *IEEE Transactions on Intelligent Transportation Systems*, vol. 20, no. 5, pp. 1883–1896, 2019.

[29] X. K. Xu, J. Peng, R. Zhang et al., "Adaptive model predictive control for cruise control of high-speed trains with time-varying parameters," *Journal of Advanced Transportation*, vol. 2019, Article ID 7261726, 11 pages, 2019.

[30] Z. Wu, X. H. Xia, and B. Zhu, "Model predictive control for improving operational efficiency of overhead cranes," *Nonlinear Dynamics*, vol. 79, no. 4, pp. 2639–2657, 2015.

[31] Q. Wang, B. Ayalew, and T. Weiskircher, "Predictive maneuver planning for an autonomous vehicle in public highway traffic," *IEEE Transactions on Intelligent Transportation Systems*, vol. 20, no. 4, pp. 1303–1315, 2019.